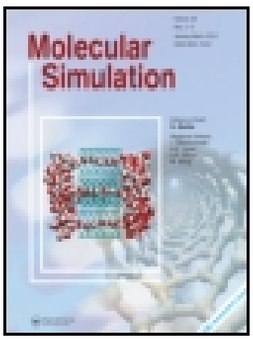

Molecular Simulation

ISSN: 0892-7022 (Print) 1029-0435 (Online) Journal homepage: https://www.tandfonline.com/loi/gmos20

Vibrational (FT-IR and FT-Raman) spectral investigations of 7-aminoflavone with density functional theoretical simulations

Y. Erdogdu , Ö. Dereli , D. Sajan , L. Joseph , O. Unsalan & M. T. Gulluoglu

To cite this article: Y. Erdogdu , Ö. Dereli , D. Sajan , L. Joseph , O. Unsalan & M. T. Gulluoglu (2012) Vibrational (FT-IR and FT-Raman) spectral investigations of 7-aminoflavone with density functional theoretical simulations, Molecular Simulation, 38:4, 315-325, DOI: 10.1080/08927022.2011.632416

To link to this article: https://doi.org/10.1080/08927022.2011.632416

Published online: 05 Dec 2011.

Molecular Simulation
Vol. 38, No. 4, April 2012, 315–325

Taylor & Francis
Taylor & Francis Group

Vibrational (FT-IR and FT-Raman) spectral investigations of 7-aminoflavone with density functional theoretical simulations

Y. Erdogdu[a], Ö. Dereli[b]*, D. Sajan[c], L. Joseph[c], O. Unsalan[d] and M.T. Gulluoglu[a]

[a]*Department of Physics, Ahi Evran University, 40040 Kirsehir, Turkey;* [b]*A. Keleşoğlu Education Faculty, Department of Physics, Selcuk University, Meram, 42090 Konya, Turkey;* [c]*Department of Physics, Bishop Moore College, Mavelikara, Alappuzha 690110, Kerala, India;* [d]*Department of Physics, Istanbul University, 34134 Istanbul, Turkey*

(*Received 5 July 2011; final version received 12 October 2011*)

FT-Raman and FT-IR spectra of the 7-aminoflavone have been recorded and analysed. The detailed interpretation of the vibrational spectra has been carried out with the aid of normal coordinate analysis following the scaled quantum mechanical force field methodology. The various intramolecular interactions that are responsible for stabilisation of the molecule were revealed by natural bond orbital analysis. The obtained vibrational wavenumbers and optimised geometric parameters were observed to be in good agreement with the experimental data. The carbonyl stretching vibrations have been lowered due to conjugation and hydrogen bonding in the molecules.

Keywords: 7-aminoflavone; FT-Raman spectra; FT-IR spectra; natural bond orbital analysis; DFT

1. Introduction

The flavones are naturally occurring heterocyclic compounds belonging to the flavonoid group. Almost all flavone derivatives have been identified from botanical sources. They are commonly found in vascular plants as phenyl-benzopyrones with different basic structures. Flavonoids are plant compounds that show biological and pharmacological activities coupled with low toxicity. Their attraction as synthetic targets is due to the wide range of biological activities they exhibit [1–4]. These plant compounds have extensive biological activities such as anti-inflammatory and anti-allergic, mutagenic and carcinogenic, and anti-HIV, and show probably protective effects against chronic diseases [5]. These include leishmanicidal activity, oviposter stimulant phytoalexins, vasodilator, antiviral, DNA cleavage, bactericidal and anticancer [6]. Some flavonoids inhibit the histamine release from human basophils and rat mast cells [7].

Aminoflavone belongs to a family of novel amino-substituted flavone derivatives. The aminoflavone and its analogue (AF) exhibit anti-proliferative activity against several renal, breast and ovarian cancer cell lines. They have shown anti-tumour activity *in vitro*, particularly against neoplastic cells of renal origin. AF was active against a number of cell lines in the NCI human tumour *in vitro* screen, including chemotherapy-resistant ovarian, renal and breast cell lines [8]. Pérez et al. [9] identified cellular correlates of responsiveness to AF in continuous human tumour renal cell carcinoma lines and in tumour cell isolates, termed renal carcinoma cell strains, from patients with clear cell and papillary renal neoplasms [8]. In addition, AF was also highly active, in the absence of specific organ toxicities, in mice bearing some of those same xenografts [10].

Flavonoids have been investigated by X-ray crystallography [11–13], electron spin resonance [14], infrared (IR) and Raman spectra [15]. Quantum chemical studies of flavonoids at semi-empirical level [16,17] as well as *ab initio* calculation at Hartree–Fock level have been reported [18,19]. This work reports a FT-IR and NIR-FT-Raman spectral study of 7-aminoflavone (7AF) to elucidate the correlation between the molecular structure and the prediction of normal modes aimed at understanding the structural and bonding features, nature of hydrogen bonding, Fermi resonance and other factors influencing the vibrational spectrum of the molecule supported by using the scaled quantum mechanical (SQM) force field technique based on density functional theory (DFT).

2. Computational details

Gaussian 03 Quantum Chemical Software was used in all calculations [20]. Molecular geometries were fully optimised by Berny's optimisation algorithm using redundant internal coordinates. All optimised structures were confirmed to be minimum energy conformations. Harmonic vibrational wavenumbers were calculated using analytic second derivatives to confirm the convergence to minima on the potential surface and to evaluate the

*Corresponding author. Email: odereli@selcuk.edu.tr

ISSN 0892-7022 print/ISSN 1029-0435 online

http://dx.doi.org/10.1080/08927022.2011.632416
http://www.tandfonline.com

zero-point vibrational energies. At the optimised structure of the 7AF, no imaginary frequency modes were obtained, proving that a true minimum on the potential energy surface (PES) was found. The optimum geometry was determined by minimising the energy with respect to all geometrical parameters without imposing molecular symmetry constraints. The optimised structural parameters and vibrational wavenumbers for all molecules were calculated by using B3LYP functional with 6-311+ +G(d,p) basis set. The assignment of bands in the vibrational spectra of molecules is an essential step in the application of vibrational spectroscopy for solving various structural–chemical problems. The SQM procedure has been widely used in the assignment of bands of vibrational spectra. In addition, the SQM method is a well-established and highly successful technique for refining computed vibrational frequencies to give much better agreement with experiment [21]. The vibrational modes were assigned on the basis of Potential Energy Distribution (PED) analysis using SQM program [22]. Normal coordinate analysis (NCA) of the title molecules was carried out to obtain a more complete description of the molecular motions involved in the fundamentals. The DFT hybrid B3LYP functional tends also to overestimate the fundamental modes in comparison with the other DFT method, therefore scaling factors have to be used for obtaining a considerably better agreement with experimental data. In this study, the calculated vibrational wavenumbers were scaled with the scale factors to figure out how the calculated data were in agreement with those of the experimental ones. The theoretical spectrum of 7AF was scaled with 0.967 (for wavenumbers fewer than 1800 cm^{-1}) and 0.955 (for those more than 1800 cm^{-1}) [1,3,23].

It should be noted that Gaussian 03 package does not calculate the Raman intensities. The Raman activities were transformed into Raman intensities using the Raint program [24] by the expression:

$$I_i = 10^{-12}\frac{(\nu_0 - \nu_1)^4}{\nu_i \cdot S}, \quad (1)$$

where I_i is the Raman intensity, S the Raman scattering activities, ν_i the wavenumber of the normal modes and υ_0 the wavenumber of the excitation laser [25].

3. Experimental

7AF sample (in powder form) was purchased from Sigma-Aldrich Chemical Company with a stated purity greater than 98% and was used as such without further purification. The IR spectrum of the sample at room temperature was recorded in the region of 4000–400 cm^{-1} on a Mattson 1000 FTIR Spectrometer calibrated using polystyrene bands (Figure 1). The sample was prepared as KBr disc. The FT-Raman spectrum of the sample was recorded in the region of 3500–50 cm^{-1} on a Bruker FRA 106/S FT-Raman instrument using 1064 nm excitation by Nd:YAG laser (Figure 2). The detector was a liquid nitrogen-cooled Ge detector.

4. Results and discussion

4.1 Conformational analysis

A fixed scan of the PES of 7AF molecule was performed at the B3LYP/6-311 + + G(d,p) level of theory along the dihedral angle C_{13}—C_{12}—C_9—O_{11}. This scan was carried out by relaxed PES scanning calculations in all geometrical parameters by changing the torsion angle for every 10°rotation around the bond. Figure 3 shows the variation of torsional barriers with the dihedral angles. While the conjugation interaction between C ring and A, B rings tends to prefer a planar structure, the steric repulsion between the ortho-ring hydrogens favours a nonplanar structure. The equilibrium geometry of the molecule results from a balance between these two effects. The dihedral angle (C_{13}—C_{12}—C_9—O_{11}) between the two planar rings and the phenyl group is 21.9197°.

Relative energies of all minima and transition state points are shown in Figure 3. The relative energy of corresponding molecules has same trends with the uniform shape of torsional dependence [1–4]. The global minimum is indicated at 20° dihedral angles (twisted conformer). Transition states are predicted at 0° (low-transition state or co-planar conformer) and 90° (high-transition state or perpendicular conformer) dihedral angles. The most stable conformer is twisted conformer. Therefore, we neglected the co-planar and perpendicular conformers in future calculations on molecular structure, vibrational spectra and natural bond orbital (NBO) analysis of the 7AF molecule.

The twisted conformer obtained equilibrium structures were then re-optimised at the B3LYP/6-311+ +G(d,p) level. The optimised molecular structure of 7AF is shown in Figure 4.

4.2 NBO analysis

NBO analysis provides an efficient method for investigating charge transfer (CT) or conjugative interaction in molecular systems. Some electron donor orbital, acceptor orbital and the interacting stabilisation energy resulting from the second-order micro disturbance theory have been reported [26]. The larger the E(2) value, the more intensive is the interaction between electron donors and electron acceptors, i.e. more donating tendency from electron donors to electron acceptors and greater the extent of conjugation of the whole system. DFT-level computation is used to investigate various second-order interactions

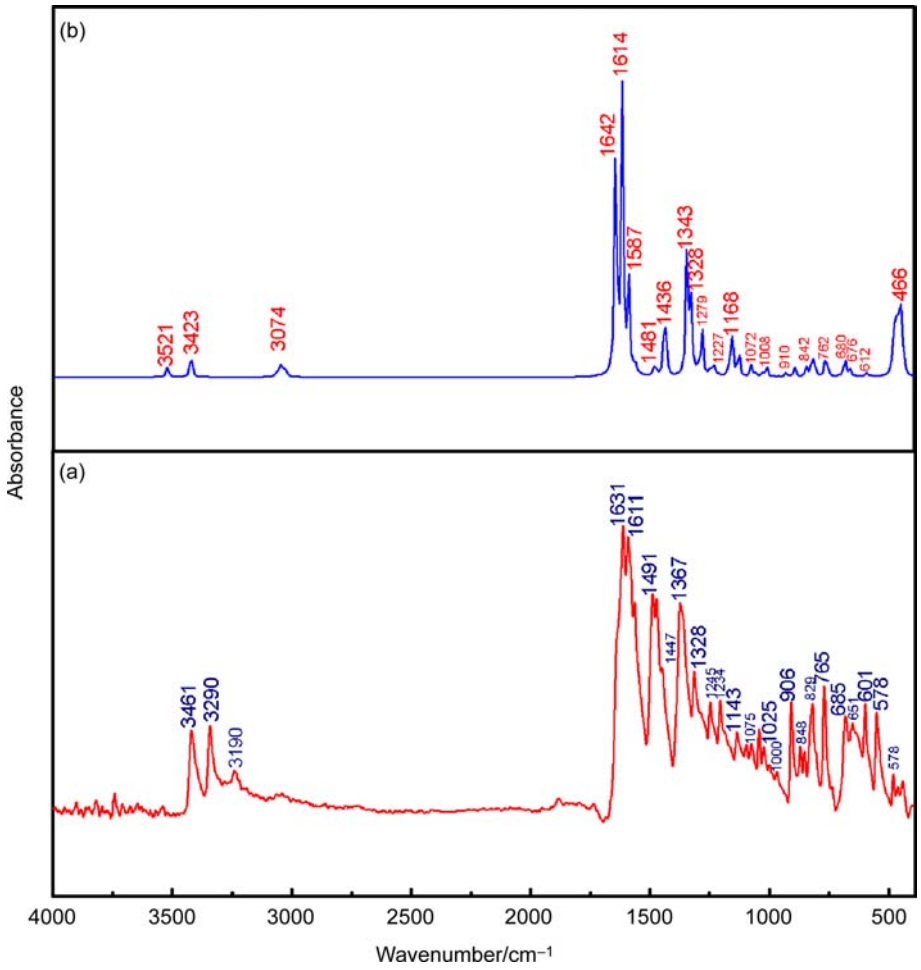

Figure 1. (Colour online) Theoretical (a) and experimental (b) FT-IR spectrum of 7AF.

between the filled orbitals of one subsystem and vacant orbitals of another subsystem, which is a measure of the delocalisation or hyperconjugation. The main natural orbital interactions were analysed with the NBO 5.0 program [27]. The hyperconjugative interaction energy was deduced from the second-order perturbation approach

$$E(2) = -n_\sigma \frac{\langle \sigma|F|\sigma\rangle^2}{\varepsilon_{\sigma^*} - \varepsilon_\sigma} = -n_\sigma \frac{F_{ij}^2}{\Delta E}, \qquad (2)$$

where $< \sigma|F|\ \sigma >^2$ or F_{ij}^2 is the Fock matrix element between the i and j NBO orbitals, ε_σ and ε_{σ^*} the energies of σ and σ^* NBO's, and n_σ the population of donor σ orbital.

The second-order perturbation theory analysis of the Fock matrix, in the NBO basis of the molecule, shows strong intramolecular hyperconjugative interactions, presented in Table 1. The intramolecular hyperconjugative interactions are formed by the orbital overlap between π (C—C) and π^* (C—C) bond orbitals, which results in intramolecular charge transfer (ICT) causing stabilisation of the system. The contributions of the stabilisation energies for the $n\,(LP_2N_{26}) \rightarrow \sigma^*\,(C_1—C_2)$ [138 kJ mol^{-1}], $n\,(LP_2\,O_{11}) \rightarrow \pi^*\,(C_9—C_8)$ [120.0 kJ mol^{-1}] and $n\,(LP_2\,O_{11}) \rightarrow \pi^*\,(C_3—C_4)$ [110.0 kJ mol^{-1}] CTs have higher values than the other delocalisations. These ICTs around the rings can induce large bioactivity in the molecule.

4.3 Vibrational analysis

The vibrational analysis of 7AF was performed on the basis of the characteristic vibrations of amino group, carbonyl and ring modes. Theoretical calculations were performed using DFT with B3LYP/6-311+ +G(d,p) basis set. The computed vibrational wavenumbers and the atomic displacements corresponding to the different normal modes are used for identifying the vibrational modes unambiguously. The calculated vibrational wavenumbers, measured IR and Raman band positions and their assignments are given in Table 2. For investigating the performance and vibrational wavenumbers for the title compound, root mean square (RMS) value between the

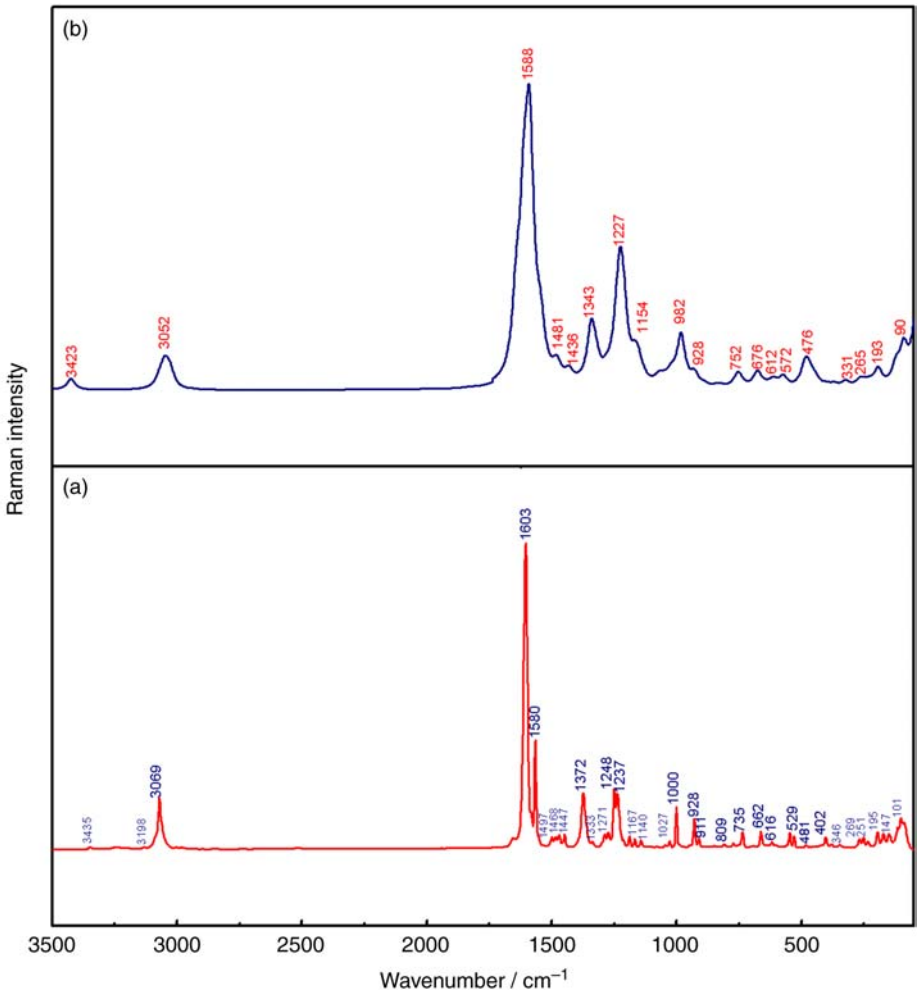

Figure 2. (Colour online) Theoretical (a) and experimental (b) FT-Raman spectra of 7AF.

calculated harmonic and observed fundamental vibrational frequencies were also calculated and are given at the bottom of the table. The RMS error of the observed (IR and Raman band) and calculated bands was found to be 32.369. Small differences between experimental and calculated vibrational modes are observed. However, deviation from the experiments is less than 10 cm^{-1} with a

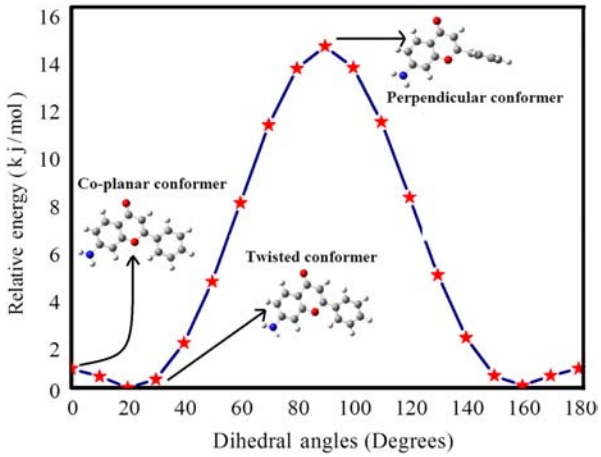

Figure 3. (Colour online) Potential energy surface scan for dihedral angle $C_{13}-C_{12}-C_9-O_{11}$.

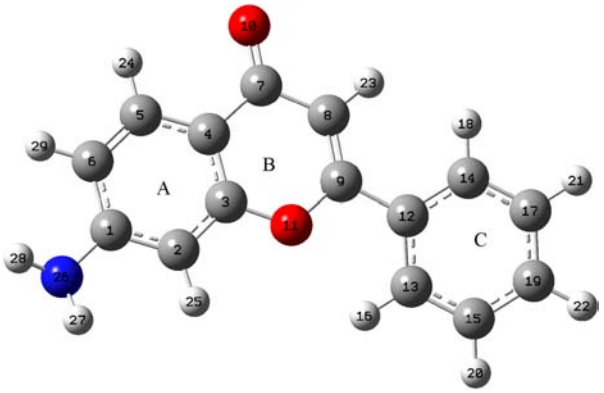

Figure 4. (Colour online) Molecular structure and atomic numbering of 7-aminoflavone.

Table 1. Second-order perturbation theory analysis of Fock matrix on NBO basis.

Lone pair	Occupancy	Donor–acceptor interaction	Hybrid (% per character)	E(2)[a] (KJ mol^{-1})	E(j)-E(i) [b] (a.u.)	F(i,j) [c] (a.u.)
LP_1O_{10}	1.9783	n (LP_1O_{10}) → σ* (C_4-C_7)	$SP^{0.68}$(40.59)	10	1.15	0.048
		n (LP_1O_{10}) → σ* (C_7-C_8)		8.7	1.44	0.044
LP_2O_{10}	1.8901	n (LP_2O_{10}) → π* (C_4-C_7)	$SP^{1.0}$(99.80)	81	0.72	0.106
		n (LP_2O_{10}) → π* (C_7-C_8)		79	0.71	0.105
LP_1O_{11}	1.9637	n (LP_1O_{11}) → σ* (C_3-C_2)	$SP^{1.68}$(62.63)	2.3	1.13	0.022
		n (LP_1O_{11}) → σ* (C_3-C_4)		26	1.14	0.075
		n (LP_1O_{11}) → σ* (C_9-C_8)		24	1.20	0.074
		n (LP_1O_{11}) → σ* (C_9-C_{12})		3.1	1.05	0.025
LP_2O_{11}	1.7637	n (LP_2O_{11}) → π* (C_3-C_4)	$SP^{1.0}$(99.90)	110	0.36	0.093
		n (LP_2O_{11}) → π* C_9-C_8)		120	0.37	0.093
LP_1N_{26}	1.8175	n (LP_2N_{26}) → σ* (C_1-C_2)	$SP^{11.70}$(92.08)	138	0.31	0.096

[a] E(2) means energy of hyperconjugative interactions; cf. Equation (1)
[b] energy difference between donor and acceptor *i* and *j* NBO orbitals
[c] *F*(*i*,*j*) is the Fock matrix element between *i* and *j* NBO orbitals.

few exceptions. This discrepancy may be due to intermolecular interactions in the solid state and the calculations may be performed in the gas phase.

4.3.1 N—H vibrations

The NH_2 group gives rise to the six internal modes of vibrations: the symmetric stretching, asymmetric stretching, symmetric deformation or scissoring, rocking, wagging and torsion modes. The symmetric stretching and asymmetric stretching modes are easily assigned owing to their characteristic magnitudes in amino-substituted benzenes. For saturated amines, it is established that the asymmetric NH_2 stretch will give rise to a band between 3450 and 3350 cm^{-1}, while the symmetric stretch will appear between 3310 and 3280 cm^{-1} [28,27]. The NH_2 asymmetric stretching mode is observed as medium band in IR spectrum at 3461 cm^{-1} and weak band in Raman at 3435 cm^{-1}. The symmetric stretching is also observed as weak band in IR spectrum at 3290 cm^{-1} and very weak band in Raman spectrum at 3244 cm^{-1}. The DFT computations give the wavenumber of these bands at 3521 cm^{-1} for NH_2 asymmetric stretch and 3423 cm^{-1} for symmetric stretch, which leads to the conclusion that substitution of electron donating group, such as NH_2 group, increases the IR intensity and decreases the stretching wavenumber due to sharing of its lone pair of electrons with the π-electrons in a ring. The movement of electron density is also justified by NBO analysis.

The scissoring mode of the NH_2 group appears in the region 1615–1650 cm^{-1} in benzene derivatives with NH_2 substituents [28–30]. The observed band in Raman spectrum at 1603 cm^{-1} is attributed to the scissoring mode of the NH_2 group, which is well supported by calculation as well (PED 64%). The C—NH_2 stretching vibrations are observed in the region 1250–1340 cm^{-1} in all the primary aromatic amines. The observed band at 1287 cm^{-1} in Raman and 1295 cm^{-1} in IR is ascribed to carbon–amine stretching. The rocking mode of the NH_2 group appears in the range 1000–1100 cm^{-1} with variable IR intensity [28]. The observed weak band at 1075 cm^{-1} in IR and at 1077 cm^{-1} in Raman spectrum attributed to the appreciable contribution from CNH angle bending, suggesting its origin due to the rocking mode. The observed band at 1044 cm^{-1} in Raman spectrum is attributed to the CNH bending mode. It is a strongly mixed mode containing contributions from the ring stretching, the planar CH deformation and the rocking modes. The wagging mode of the NH_2 group appears in the range 600–850 cm^{-1}. The observed weak bands at 346 cm^{-1} in Raman spectrum is assigned to the torsion mode of amino group vibration. The wavenumber observed at 467 cm^{-1} in IR is assigned to C—NH_2 in-plane bending mode.

4.3.2 C—O vibrations

The carbonyl bands are the most characteristic bands of the IR and Raman spectra, and for this reason such bands have been the subject of extensive studies [28–30]. The intensity of C = O stretch increases due to conjugation or the formation of hydrogen bonds. The increase in conjugation therefore leads to intensification of Raman lines as well as increased IR band intensities. In 7AF, the C—O bond is conjugated with the γ-pyrone ring. The carbonyl stretching wavenumber of flavones is observed in the range 1670–1625 cm^{-1}[1–4,14,15,19]. The intense band at 1631 cm^{-1} in the IR spectrum can be assigned to the C_7 = O_{10} stretch. The results of computations give the wavenumber of this mode to be 1642 cm^{-1}. This decrease can be explained by an increase in the π-conjugation between the B ring and pyrone part through the inter-ring bond. The torsion angle between the side phenyl group and the rest of the molecule strongly influence the π-electron distribution. In the solid state, the dihedral angle is smaller due to the constraints induced by the effect of intermolecular interaction in the crystal, which results in

Table 2. Experimental and calculated [B3LYP/6-311++G(d,p)] wavenumbers of 7AF and potential energy distributions of vibrational modes.

Mode description	Calc.[a]	Scaled[b]	I^{c}_{IR}	I^{d}_{Raman}	Exp. IR	Exp. Raman	TED[e] (%)
Torsion (B-C)	36	35	0.12	40.5	–	–	$T_{O11C9C12C13}(87)$
o.p. COCC bending (AB-C)	57	55	0.10	4.70	–	–	$\gamma_{C4C2O11C3} + \gamma_{C9C13C14C12} + T_{C1C2C3C4} + T_{C2C3O11C9} + T_{C3O11C9C12}(74)$
OCC bending (AB-C)	93	90	0.11	15.6	–	87 vw	$\beta_{C12C9O11}(65) + \beta_{C9C12C14}(18)$
Ring torsion (A-B)	105	101	0.08	1.42	–	101 m	$T_{C2C3C4C5} + T_{C2C3O11C9} + T_{C1C2C3C4} + T_{C3C4C5C6}(70)$
Ring torsion (B)	127	122	0.71	8.39	–	147 w	$T_{C1C2C3C4} + T_{C2C3C4C5} + T_{C2C3O11C9} + T_{C7C8C9C12}\ T_{C2C3C4C5} + T_{C2C3O11C9} + T_{C3O11C9C12} + T_{C13C15C19C17}\ (65) + \gamma_{C4C2O11C3} + \gamma_{C9C13C14C12}(11)$
Ring torsion (B)	200	193	0.29	8.22	–	195 w	$T_{C3O11C9C12} + T_{C7C8C9C12} + T_{C13C15C19C17}(49) + \gamma_{C9C13C14C12}(10)$
CCO bending (AB)	236	229	0.44	1.90	–	232 vw	$\beta_{C2C3O11} + \beta_{C3O11C9} + \beta_{C8C7O10} + \beta_{C8C9O11} + \beta_{C12C9O11}\ (38) + \beta_{C9C12C14} + \beta_{C6C1N26} + \beta_{C2C3O11} + \beta_{C4C5C6}\ (15)$
Ring torsion (A)	259	250	0.50	1.41	–	251 vw	$T_{C1C2C3C4} + T_{C2C3C4C5}(33) + T_{C2C3O11C9}(22) + \gamma_{N26C2C6C1}(10)$
CC stretching (AB-C)	274	265	0.02	2.70	–	269 vw	$\nu_{C9C12}(25) + \beta_{C3O11C9} + \beta_{C4C5C6} + \beta_{C7C8C9} + \beta_{C8C9O11} + \beta_{C15C19C17}\ (13) + \beta_{C12C13C15}(14)$
Ring torsion (AB)	290	280	0.49	0.38	–	–	$T_{C2C3C4C5} + T_{C2C3O11C9} + T_{C3O11C9C12} + T_{C13C15C19C17}(53)$
i.p. OCC bending (B)	334	323	1.15	2.62	–	–	$\beta_{C2C3O11} + \beta_{C8C7O10} + \beta_{C8C9O11} + \beta_{C12C9O11}(34)$
CCNH torsion	342	331	2.46	0.35	–	346 vw	$T_{H27N26C1C2} + T_{H28N26C1C2}(90)$
i.p. NCC bending	381	369	0.21	1.56	–	–	$\beta_{C6C1N26}(33) + \beta_{C3C4C5}(25)$
Ring torsion (C)	412	399	0.02	1.25	–	402 w	$T_{C13C15C19C17} + T_{C14C17C19C15}(79) + T_{H16C13C15C19} + T_{H18C14C17C19} + T_{H20C15C19C17} + T_{H21C17C19C15}(16)$
Ring torsion (A)	450	435	6.62	1.11	–	–	$T_{C3C4C5C6} + T_{H27N26C1C2} + T_{H28N26C1C2}(38) + \gamma_{C4C2O11C3} + \gamma_{N26C2C6C1}(28)$
CCNH torsion	464	449	40.2	3.25	–	–	$T_{H27N26C1C2} + T_{H28N26C1C2} + T_{H27N26C1C2} + T_{H28N26C1C2}(35) + \gamma_{C4C2O11C3} + \gamma_{N26C2C6C1} + \gamma_{C9C13C14C12}\ (15)$
Ring torsion (A)	482	466	18.2	1.57	467 vw	–	$T_{H28N26C1C2} + T_{H27N26C1C2}(47) + T_{C3C4C5C6}\ (11) + \gamma_{N26C2C6C1}(10)$
Ring bending (A-B)	492	476	13.0	7.66	481 w	481 vw	$\beta_{C2C3O11} + \beta_{C3C4C5} + \beta_{C4C5C6} + \beta_{C1C2C3} + \beta_{C2C3O11} + \beta_{C3O11C9} + \beta_{C7C8C9} + \beta_{C8C7O10} + \beta_{C8C9O11} + \beta_{C12C9O11}\ (31)\ T_{H27N26C1C2} + T_{H28N26C1C2} + \gamma_{C9C13C14C12} + T_{C14C17C19C15}(16)$
Ring bending (A-B)	506	490	0.55	6.79	503 m	529 w	$\beta_{C2C3C4} + \beta_{C3O11C9} + \beta_{C7C8C9} + \beta_{C8C9O11}(56)$
Ring bending (A-B)	591	572	0.33	4.84	578 vw	–	$\beta_{C2C3C4} + \beta_{C4C5C6} + \beta_{C13C15C19} + \beta_{C14C17C19}(48)$
i.p. CC=O bending	609	589	1.41	0.44	–	–	$\beta_{C1C2C3} + \beta_{C2C3O11} + \beta_{C8C7O10} + \beta_{C15C19C17}(64)$
Ring bending (C)	633	612	0.07	2.05	601 m	616 vw	$\beta_{C13C15C19} + \beta_{C14C17C19}(72)$
o.p. CCOC torsion	634	613	0.22	1.41	–	–	$\gamma_{C4C2O11C3} + \gamma_{N26C2C6C1}(70)$
o.p. CCOC torsion	660	638	0.36	0.75	–	–	$T_{C12C13C15C19}(19)\ \gamma_{O10C4C8C7}(17)\ \gamma_{C8C12O11C9}(30)$
o.p. CCOC torsion	681	659	2.74	0.38	651 w	662 m	$\gamma_{O10C4C8C7}(12)\ \gamma_{C8C12O11C9}(25)\ T_{C1C2C3C4} + T_{C3C4C5C6}(25)$
Ring bending (C)	699	676	0.67	6.88	673 vw	–	$\beta_{C15C19C17} + \beta_{C14C17C19} + \beta_{C13C15C19}(55)$
CCCH torsion (C)	703	680	6.79	0.47	685 m	689 w	$T_{H20C15C19C17} + T_{H22C19C17C14} + T_{H18C14C17C19} + T_{H16C13C15C19}(54) + T_{C12C13C15C19}(33)$
i.p. CC-O bending	729	705	0.40	0.22	–	–	$\beta_{C8C9O11} + \beta_{C1C2C3}(43) + \nu_{C5C4} + \nu_{C1C2} + \nu_{C8C9}(10)$
o.p. CCC=O bending	758	733	0.07	0.42	–	735 w	$\gamma_{O10C4C8C7}(29) + T_{H29C6C1N26} + T_{H24C5C6C1} + T_{H23C8C9C12}\ (22) + T_{C1C2C3C4} + T_{C3C4C5C6}(14)$
Ring bending (A-B)	777	752	3.16	5.86	–	–	$\beta_{C2C3O11} + \beta_{C3C4C5} + \beta_{C4C5C6}(12) + \nu_{C5C6} + \nu_{C1C2} + \nu_{C3C4}(10)$
CCCH torsion (C)	788	762	6.43	1.34	765 m	770 vw	$T_{H20C15C19C17} + T_{H22C19C17C14} + T_{H18C14C17C19} + T_{H16C13C15C19}(24) + T_{C12C13C15C19}(13)$
NCCH torsion	831	804	2.40	0.05	–	809 vw	$T_{H29C6C1N26}(60) + T_{H24C5C6C1}(11)$
NCCH torsion	844	816	8.64	0.12	–	–	$T_{H25C2C1N26}(75)$
CCCH torsion (C)	855	826	0.35	1.07	829 m	–	$T_{H16C13C15C19} + T_{H18C14C17C19} + T_{H20C15C19C17} + T_{H21C17C19C15}(90)$

Table 2 – *continued*

Mode description	Calc.[a]	Scaled[b]	I^{c}_{IR}	I^{d}_{Raman}	Exp. IR	Exp. Raman	TED[e] (%)
CCCH torsion (B)	870	842	3.30	0.53	848 w	845 vw	$\gamma_{O10C4C8C7}(71) + T_{H23C8C9C12}(13)$
Ring bending (B)	919	888	3.52	1.09	–	–	$\beta_{C3O11C9} + \beta_{C4C5C6} + \beta_{C7C8C9} + \beta_{C8C9O11} + \beta_{C15C19C17}(28) + \nu_{C15C19} + \nu_{C17C19} + \nu_{O11C9}(14)$
CCCH torsion (C)	941	910	0.28	0.07	906 m	911 w	$T_{H16C13C15C19} + T_{H18C14C17C19} + T_{H22C19C17C14}(87)$
Ring bending (A)	960	928	1.41	5.65	–	928 m	$\beta_{C2C3C4} + \beta_{C3C4C5} + \beta_{C4C5C6}(31) + \nu_{O11C3}(10)$
CCCH torsion (A)	987	955	0.18	0.04	–	–	$T_{H24C5C6C1} + T_{H29C6C1N26}(77)$
CCCH torsion (C)	991	958	0.07	0.16	–	–	$T_{H16C13C15C19} + T_{H18C14C17C19} + T_{H20C15C19C17} + T_{H21C17C19C15}(83) + T_{C13C15C19C17} + T_{C14C17C19C15}(15)$
CCCH torsion (C)	1006	973	0.03	0.11	–	969 vw	$T_{H22C19C17C14} + T_{H20C15C19C17} + T_{H21C17C19C15}(67)$
Ring bending (C)	1016	982	0.19	23.7	–	–	$\beta_{C13C15C19} + \beta_{C14C17C19} + \beta_{C15C19C17}(53) + \nu_{C13C15} + \nu_{C14C17+} \nu_{C15C19} + \nu_{C17C19}(34)$
Ring stretching (C)	1042	1008	3.58	1.13	1000 vw	1000 s	$\nu_{C15C19} + \nu_{C17C19}(40)$
CC Stretching, CCH bending (C)	1058	1023	1.28	4.76	1025 w	1027 m	$\nu_{C15C19} + \nu_{C17C19}(24)\ \beta_{H16C13C15} + \beta_{H18C14C17} + \beta_{H20C15C19} + \beta_{H21C17C19}(16)\ \beta_{C13C15C19} + \beta_{C14C17C19} + \beta_{C15C19C17}(13)$
CNH bending	1089	1053	1.00	2.28	–	1044 w	$\beta_{H27N26C1}(44)$
CCH bending (C)	1107	1070	0.18	0.24	–	–	$\beta_{H16C13C15} + \beta_{H20C15C19} + \beta_{H22C19C17}(33) + \nu_{C13C15}(19)$
CC Stretching, CNH bending	1108	1072	4.29	2.89	1075 w	1077 vw	$\nu_{C7C8}(14) + \beta_{H27N26C1}(12)$
Ring stretching (A)	1163	1125	10.1	0.62	–	–	$\nu_{C1C2} + \nu_{C3C4} + \nu_{C5C6}(67)$
CCH bending (C)	1185	1146	0.02	1.55	1143 m	1140 m	$\beta_{H20C15C19} + \beta_{H21C17C19} + \beta_{H22C19C17}(82)$
C-O stretching	1193	1154	19.7	7.05	–	1167 m	$\nu_{O11C3}(45) + \beta_{H25C2C1}(21)$
CCH bending (C)	1208	1168	1.92	8.03	1185 vw		$\beta_{H16C13C15} + \beta_{H18C14C17} + \beta_{H20C15C19} + \beta_{H21C17C19}(75) + \nu_{C13C15} + \nu_{C14C17}(16)$
Ring stretching (A-B)	1252	1211	0.62	20.8	–	1212 vw	$\nu_{C5C4} + \nu_{C1C2} + \nu_{C8C9} + \nu_{C9C12} + \nu_{C5C4} + \nu_{C1C2} + \nu_{C8C9}(43)$
CCH bending (A-B)	1268	1227	3.37	44.6	1234 m	1237 s	$\nu_{C9C12}(13) + \beta_{H23C8C9} + \beta_{H25C2C1}(35)$
CCH bending (C)	1285	1242	3.91	11.4	1245 m	1248 s	$\beta_{H18C14C17} + \beta_{H16C13C15} + \beta_{H20C15C19}(22)$
Ring stretching (B-C)	1322	1279	19.0	3.38	–	1271 m	$\nu_{C12C9}(24) + \nu_{N26C1} + \nu_{N26C1} + \nu_{O11C3} + \nu_{O11C3}(21)$
CCH bending (A)	1338	1293	2.61	0.09	1295 vw	1287 w	$\nu_{N26C1} + \nu_{O11C3}(18)\ \beta_{H24C5C6} + \beta_{H29C6C1}(24)$
CCH bending (C)	1356	1312	2.23	1.04	–	–	$\beta_{H18C14C17} + \beta_{H16C13C15} + \beta_{H20C15C19}(56) + \nu_{C13C15} + \nu_{C12C13} + \nu_{C17C19}(35)$
Ring stretching (A-C)	1373	1328	33.7	8.70	1328 m	1333 w	$\nu_{C5C6} + \nu_{C1C2} + \nu_{C3C4+}\nu_{C15C19} + \nu_{C17C19}(37) + \nu_{O11C9}(12)$
Ring stretching (A-B)	1388	1343	45.0	23.4	1367 s	1372 s	$\nu_{C5C6} + \nu_{C1C2} + \nu_{C3C4}(23)$
CCH bending (C)	1478	1429	4.59	3.63	–	–	$\beta_{H16C13C15} + \beta_{H20C15C19} + \beta_{H22C19C17}(51) + \nu_{C13C15}(13)$
Ring stretching (A-B)	1485	1436	25.8	1.43	1447 m	1447 m	$\nu_{C1C2} + \nu_{C3C4} + \nu_{C5C6} + \nu_{C2C3} + \nu_{C5C4} + \nu_{C8C9}(41) + \beta_{H24C5C6} + \beta_{H29C6C1}(13)$
CCH bending (C)	1525	1474	3.11	2.18	–	1468 m	$\beta_{H16C13C15} + \beta_{H18C14C17} + \beta_{H20C15C19} + \beta_{H21C17C19}(61) + \beta_{C13C15C19} + \beta_{C14C17C19} + \beta_{C15C19C17}(12)$
CCH bending (A)	1532	1481	1.65	5.73	1491 s	1497 w	$\beta_{H24C5C6} + \beta_{H29C6C1}(29) + \beta_{C2C3O11} + \beta_{C3C4C5} + \beta_{C4C5C6}(11)$
Ring stretching (A-B)	1597	1544	0.57	19.2	–	–	$\nu_{C1C2} + \nu_{C3C4} + \nu_{C8C9}(48)$
Ring stretching (B-C)	1614	1560	5.03	4.72	–	1565 vw	$\nu_{C8C9} + \nu_{C15C19} + \nu_{C17C19} + \nu_{C12C13}$ (57)
Ring stretching (A-B)	1641	1587	23.2	2.36	1588 s	1580 s	$\nu_{C1C2} + \nu_{C8C9}(34)$
Ring stretching (C)	1643	1588	11.0	100	–	–	$\nu_{C13C15} + \nu_{C14C17} + \nu_{C15C19} + \nu_{C17C19}(63)\ \beta_{H16C13C15} + \beta_{H18C14C17} + \beta_{H20C15C19} + \beta_{H21C17C19}(15)$
HNH bending	1658	1604	3.14	21.4	–	1603 vs	$\beta_{H28N26H27}(64)$
Ring stretching (A)	1669	1614	100	50.4	1611 vs	–	$\nu_{C1C2} + \nu_{C3C4} + \nu_{C5C6}(34) + \beta_{H28N26H27}(15)$
C=O stretching	1698	1642	89.4	32.7	1631 vs	–	$\nu_{O10C7}(71)$
CH stretching (A)	3166	3024	2.45	3.40	–	–	$\nu_{C6H29}(95)$

Table 2 – *continued*

Mode description	Calc.[a]	Scaled[b]	I^{c}_{IR}	I^{d}_{Raman}	Exp. IR	Exp. Raman	TED[e] (%)
CH stretching (C)	3167	3024	0.07	1.01	–	–	$\nu_{C15H20} + \nu_{C17H21} + \nu_{C19H22}(94)$
CH stretching (C)	3176	3033	1.43	3.13	–	–	$\nu_{C15H20} + \nu_{C17H21}(88)$
CH stretching (A)	3183	3040	0.78	1.43	–	–	$\nu_{C2H25}(99)$
CH stretching (C)	3187	3044	3.64	3.57	–	–	$\nu_{C14H18} + \nu_{C15H20} + \nu_{C19H22}(89)$
CH stretching (C)	3196	3052	1.73	3.61	–	3069 m	$\nu_{C14H18} + \nu_{C17H21} + \nu_{C19H22}(84)$
CH stretching (A)	3197	3053	0.97	2.58	–		$\nu_{C5H24}(94)$
CH stretching (C)	3208	3063	0.68	2.09			$\nu_{C13H16}(91)$
CH stretching (B)	3219	3074	0.35	2.30	3190 vw	3198 vw	$\nu_{C8H23}(97)$
NH stretching	3584	3423	10.1	5.22	3290 w	3244 vw	$\nu_{N26H27} + \nu_{N26H28}(100)$
NH stretching	3687	3521	4.40	0.99	3461 m	3435 w	$\nu_{N26H27} + \nu_{N26H28}(100)$
RMS		32.369					

A, B, C: Rings; *ν*: Stretching; γ: out-of-plane bending; β: in-plane bending; T: Torsion; *vs*: very strong; s: strong; m: medium; w: weak; vw: very weak.

[a] Unscaled calculated wavenumbers.

[b] Obtained from the wave numbers calculated at B3LYP/6-31++G(d,p) using scaling factors 0.967 (for wave numbers fewer than 1800 cm^{-1}) and 0.955 (for those more than 1800 cm^{-1}).

[c] Relative absorption intensities normalised with highest peak absorption equal to 100.

[d] Relative Raman intensities normalised to 100. [e] Total energy distribution calculated B3LYP/6-311++G(d,p) level of theory. Only contributions ≥10% are listed.

a stronger π-electron delocalisation [1–4,19]. Hence the lowering of the carbonyl stretching mode can be attributed to the conjugation, which is justified by DFT calculations. The strong intense bands at 1328 cm^{-1} in IR and 1333 cm^{-1} in Raman spectrum are attributed to the C—C and C—O stretching mode. The C = O in-plane and out-of-plane bending modes are coupled with other modes.

4.3.3 Chromone part C = C vibrations

The C = C stretching vibration of flavone derivatives is expected around 1619 cm^{-1} [1–4]. The DFT calculation gives the wavenumber at 1614 cm^{-1}. The intense bands in IR spectrum at 1611 cm^{-1} are predominantly localised on the $C_8 = C_9$ double bond of the chromone part, which is coupled with NH_2 in-plane bending mode. This bond length is clearly shorter than all other C—C bonds and behaves like a real double bond, which is well supported by $C_8 = C_9$ bond lengths of similar flavone derivatives [1–4]. The medium band at about 1271 cm^{-1} in Raman spectra corresponds to C_9—C_{12} stretching vibrations and its high intensity is due to mechanical coupling with other ring vibrations [1–4,14,15,19]. The wavenumber increase of the C_9—C_{12} vibrations for the crystalline state suggests that the molecule must be planar. Indeed, for a planar structure, the delocalisation of π-electron throughout the whole molecule, and particularly across the C—C inter-ring bond, is more pronounced than for a twisted molecule; this delocalisation affects the bond length of the C_9—C_{12} bond, which must have a more marked double bond character and so a high wavenumber. Another wavenumber modification is observed in the IR spectrum of 7AF in the solid state for the mode 9a of ring C, which appears at 1234 cm^{-1} and in the corresponding Raman spectrum at 1237 cm^{-1}. For a planar structure, this in-plane vibrational mode must be affected by important steric interaction between ortho-hydrogen (H_{23} and H_{18}) of the ring B and H_{16} and the pair of non-bonding electrons O_{11}.

4.3.4 Phenyl ring modes

The normal vibrations of the benzene ring are usually described in terms of Wilson numbers [31]. In 7AF the ring C is mono-substituted benzene. The actual band positions of the ring stretching vibrations are determined by the form of constituents around the ring [28–30]. The two doubly degenerate ring stretching modes 8a and 8b (1600 cm^{-1}) and 19a and 19b (1490 cm^{-1}), and the two non-degenerate modes of benzene 14 (1300 cm^{-1} and 998 cm^{-1}) correspond to C—C skeletal vibrations [31]. The phenyl ring mode 8a manifests as very intense bands in IR and Raman spectra at 1588 cm^{-1} and 1580 cm^{-1}, respectively. Its relatively weaker companion 8b is observed at 1565 cm^{-1} in Raman spectra. The wavenumber of vibration 19 in mono-substituted benzene

derivative is insensitive to substitution. This 19a mode can be expected in the range 1470–1515 cm^{-1} with higher intensity and 19b in the range 1440–1470 cm^{-1} as weak band [28–30]. The modes corresponding to 19a are observed at 1491 cm^{-1} in IR and at 1497 cm^{-1} in Raman spectrum. Mode 19b can be observed as a medium band at 1447 cm^{-1} both in IR and Raman spectra.

The ring breathing vibrations are generally very strong in Raman spectrum. Normal vibration 1 of phenyl ring is usually referred to as a substituent sensitive vibration. For a heavy substitution these modes found in the region 1100–1000 cm^{-1} are strongly Raman active [28–30]. This is confirmed by the strong intense Raman band at 1027 cm^{-1} and weak intense IR band at 1025 cm^{-1}, which are supported by computed results. The in-plane ring deformation or trigonal ring breathing vibration derived from the b_{1u} benzene vibration 12 (1010 cm^{-1}) gives rise to an intense Raman band in mono-substituted benzene [28–30] at 1010–990 cm^{-1}. In benzene this vibration is essentially a contraction of the ring at the triangle formed by the 1, 3, 5 carbon atoms, accompanied by an expansion of the ring at the triangle formed by the 2, 4, 6 carbon atoms. This mode is termed as Star of David Vibration, upon mono-substitution the motion of the two triangles is decoupled and the vibrational amplitudes at positions 1, 3 and 5 are damped. In 7AF the vibrational mode 12 is identified as a strong intense Raman band at 1000 cm^{-1} and very weak band in IR spectrum at 1000 cm^{-1}, which is also supported by computed results.

4.3.5 C—H vibrations

The aromatic C—H stretching [28–30] vibrations in mono-substituted benzene rings are generally observed in the region 3000–3100 cm^{-1}. The C—H stretching vibrations in the benzene derivatives arise from two non-degenerate modes a_{1g} (3072 cm^{-1}) and b_{1u} (3060 cm^{-1}), and two degenerate mode e_{2g} (3047 cm^{-1}) and e_{1u} (3099 cm^{-1}), i.e. vibrations 2, 13, 7 and 20, respectively. The medium intense Raman band at 3069 cm^{-1} is assigned to mode 2 of benzene, which corresponds to the aromatic C—H stretching of the mono-substituted C ring.

The ring stretching vibration of chromone part in 7AF is observed as very weak band at 1212 cm^{-1} in Raman and the corresponding calculated value is 1211 cm^{-1}. The out-of-plane C_4-H_{11} bend is observed at 848 cm^{-1} and 845 cm^{-1} in IR and Raman spectra, respectively, is well supported by the computed values of chromone part. The C—H in-plane bending [28–30] vibrations appear in the region 1300–1000 cm^{-1}. The vibrational mode 18a could be identified in 7AF as a weaker band in both Raman and IR spectrum at 1140 and 1143 cm^{-1}, respectively, which is a characteristic vibration of mono-substituted phenyl ring. The phenyl ring mode 9a could be identified as medium bands in the region of ring stretching vibrations at 1271 cm^{-1} in Raman spectrum and 9b are found in IR at 1185 cm^{-1}. The absorption bands arising from C—H out-of-plane bending vibrations are usually observed in the region [28–30] 1000–675 cm^{-1}. The vibrational mode 4 occurs as a medium IR band at 685 cm^{-1} but is a weak band in the Raman at 689 cm^{-1}. For mono-substituted benzenes another ring deformation derived from benzene vibration 6b (606 cm^{-1}) gives rise to a medium intense IR band at 673 cm^{-1}. Ring deformation 6a can be found as a medium band at 601 cm^{-1} in IR and as a weak band at 616 cm^{-1} in Raman spectrum.

4.4 HOMO–LUMO analysis

The HOMO (highest occupied molecular orbital)–LUMO (lowest unoccupied molecular orbital) energy gap for 7AF was computed at the B3LYP/6-311++G(d,p) level. The eigenvalues of LUMO (− 1.985 eV) and HOMO (− 6.226 eV) and their energy gap (4.241eV) reflect the chemical activity of the molecule, which influences the biological activity of the molecule. The atomic orbital compositions of the frontier molecular orbitals are shown in Figure 5.

The HOMO energy directly correlates with the ionisation potential in a molecule and characterises the susceptibility of the molecule towards attack by electrophiles. The LUMO energy correlates directly with electron affinity and characterises the susceptibility of the molecule towards attack by a nucleophile. Both the HOMO and LUMO energies are important in radical reactions [32].

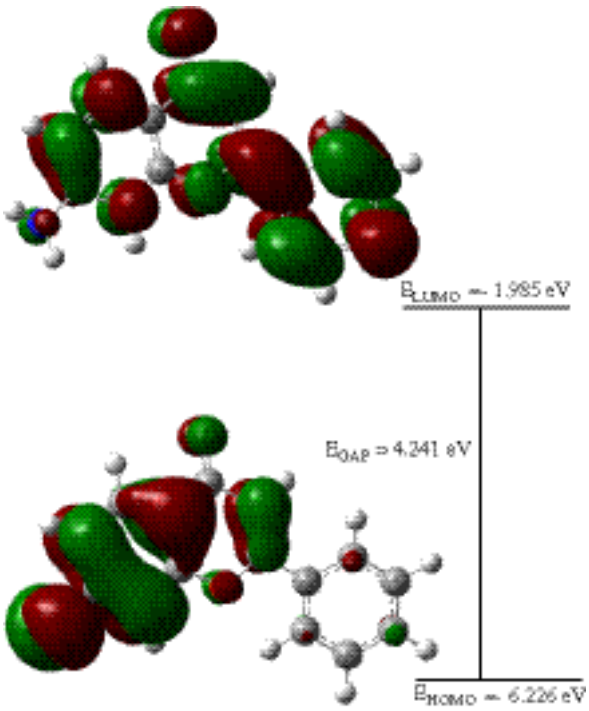

Figure 5. (Colour online) HOMO and LUMO plots of 7-aminoflavone.

The HOMO–LUMO gap, i.e. the difference in energy between the HOMO and LUMO, is an important stability index [33]. A large HOMO–LUMO gap implies high stability for the molecule with respect to further chemical reaction [34]. Thus, a large HOMO–LUMO energy gap can be considered as an indicator of higher stability of a compound towards a chemical reaction, especially in the case of radical reactions.

The peculiar features observed in Raman and IR spectra are simultaneous activation of some of the vibrational modes. The experimental behaviour is well accounted for by *ab initio* calculations in π-conjugated molecules that predict exceptionally large Raman cross-sections and IR intensities for the same normal modes. The simultaneous IR and Raman activation of the ring stretching mode, carbonyl stretching and the aromatic C—H in-plane bending mode gives the evidence of ICT between the C = O and NH_2 groups through conjugated ring path and is responsible for bioactivity of the molecule.

5. Conclusions

In recent years, DFT has become a powerful tool in the investigation of molecular structures and vibrational spectra, especially B3LYP method has been widely used [35–39]. In this study, the NCA performed by B3LYP method on 7AF reproduces its experimental geometry and, according to the RMS value, there is an excellent agreement between experimental and predicted wavenumbers. The simultaneous occurrence of ring stretching mode, carbonyl stretching and the aromatic C—H in-plane bending mode provides evidence for the CT interactions that are responsible for the bioactivity of the molecule. The lowering of NH_2 stretching wavenumber is due to the hyperconjugation interaction between the n (LP_2N_{26}) σ^* (C_1—C_2) bond and is confirmed by NBO analysis. The red shifting of C = O stretching wavenumbers is due to the conjugation between carbonyl groups and the γ-pyrone ring.

Acknowledgements

This work was supported by the research fund of Ahi Evran University (Project no. A10/2009) and BAP office of Selcuk University (Project no. 11401012). The authors would like to thank the central laboratory of METU (ODTÜ) for recording FT-Raman spectra, Gazi University Art and Science Faculty Department of Chemistry for recording FT-IR spectra and associate professor Dr Mustafa Kurt for the Gaussian 03W program package.

References

[1] Y. Erdogdu, O. Unsalan, D. Sajan, and M.T. Gulluoglu, *Structural conformations and vibrational spectral study of chloroflavone with density functional theoretical simulations*, Spectrochim. Acta A 76 (2010), pp. 130–136.

[2] Y. Erdogdu, O. Unsalan, and M.T. Gulluoglu, *Vibrational analysis of Flavone*, Turk. J. Phys. 33 (2009), pp. 249–259.

[3] Y. Erdogdu, O. Unsalan, and M.T. Gulluoglu, *FT-Raman, FT-IR spectral and DFT studies on 6, 8-Dichloroflavone and 6, 8-Dibromoflavone*, J. Raman Spectros. 41(7) (2010), pp. 820–828.

[4] O. Unsalan, Y. Erdogdu, and M.T. Gulluoglu, *FT-Raman and FT-IR spectral and quantum chemical studies on some Flavonoid derivatives: Baicalein and Naringenin*, J. Raman Spectros. 40(5) (2009), pp. 562–570.

[5] H. Böhm, J. Boeing, J. Hempel, B. Raab, and A. Kroke, *Flavonols, flavones annd anthocyanins as natural antioxidants of food and their possible role in the prevention of chronic diseases*, Z. Ernährungswiss 37 (1998), pp. 147–163.

[6] J.A. Seijas, M.P. Vazques-Tato, and R.C. Reboredo, *Solvent-free synthesis of functionalized flavones under microwave irradiation*, J. Org. Chem. 70 (2005), pp. 2855–2858.

[7] S. Yano, H. Tachibana, and K. Yamada, *Flavones suppress the expression of the high-affinity IgE receptor FcεRI in human basophilic KU812 cells*, J. Agric. Food Chem. 53 (2005), pp. 1812–1817.

[8] M.J. Kuffel, J.C. Schroeder, L.J. Pobst, S. Naylor, J.M. Reid, S.H. Kaufmann, and M.M. Ames, *Activation of the antitumor agent aminoflavone (NSC 686288) is mediated by induction of tumor Cell Cytochrome P450 1A1/1A2*, Mol. Pharmacol. 62 (2002), pp. 143–153.

[9] A.I.L. Pérez, S. Kenney, J. Boswell, M. Hollingshead, C. Hose, W.M. Linehan, R. Worrell, L. Rubinstein, E.A. Sausville, and D.T. Vistica, *Sensitivity of renal cell carcinoma to aminoflavone: role of CYP1A*, J. Urol. 171 (2004), pp. 1688–1697.

[10] M.C. Alley, S.F. Stinson, C.M. Pacula-Cox, R.F. Camalier, L.R. Phillips, T.W. Daw, and E.A. Sausville, *Pharmacologic evaluations of a novel amino-substituted flavone (NSC 686288) exhibited unique in vitro and in vivo anticancer activities*, Proc. Am. Assoc. Cancer Res. 40 (1999), pp. 119–128.

[11] S.A. van Acker, M.J. de Groot, D.J. van den Berg, M.N. Tromp, G. Donne-Op den Kelder, W.J. van der Vigh, and A. Bast, *A quantum chemical explanation of the antioxidant activity of flavonoids*, Chem. Res. Toxicol. 9 (1996), pp. 1305–1312.

[12] M. Shoja, *5-Hydroxyflavone*, Acta Crystallogr. 46 C (1990), pp. 517–519.

[13] J. Seetharaman and S.S. Rajan, *Structure of 6-hydroxyflavone*, Acta Crystallogr. 48C (1992), pp. 1714–1715.

[14] J.P. Cornard, J.C. Merlin, A.C. Boudet, and L. Vrielynck, *Structural study of quercetin by vibrational and electronic spectroscopies combined with semiempirical calculations*, Biospectroscopy 3 (1997), pp. 183–193.

[15] L. Vrielynck, J.P. Cornard, and J.C. Merlin, *Semi-empirical and vibrational studies of flavone and some deuterated analogues*, Spectrochim. Acta A 50 (1994), pp. 2177–2188.

[16] G.K. Pereira, P.M. Donate, and S.E. Galemeck, *Electronic structure of hydroxylated derivatives of flavylium cation*, J. Mol. Struct. (Theochem) 363 (1996), pp. 87–96.

[17] G.K. Pereira, P.M. Donate, and S. Galemeck, *Effects of substitution for hydroxyl in the B-ring of the flavylium cation*, J. Mol. Struct. (Theochem) 392 (1997), pp. 169–179.

[18] H.M. Ishiki, P.M. Donate, and S.E. Galemeck, *Electronic structure of chromone and its hydroxylated derivatives on positions 2 and 3*, J. Mol. Struct. (Theochem) 423 (1998), pp. 235–243.

[19] J.P. Abraham, D. Sajan, J. Mathew, I.H. Joe, V. George, and V.S. Jayakumar, *Structural conformations and electronic interactions of the natural product, oroxylin: a vibrational spectroscopic study*, J. Raman Spectrosc. 39 (2008), pp. 1821–1831.

[20] M.J. Frisch, G.W. Trucks, H.B. Schlegel, G.E. Scuseria, M.A. Robb, J.R. Cheeseman, J.A. Montgomery, Jr., T. Vreven, K.N. Kudin, J.C. Burant, J.M. Millam, S.S. Iyengar, J. Tomasi, V. Barone, B. Mennucci, M. Cossi, G. Scalmani, N. Rega, G.A. Petersson, H. Nakatsuji, M. Hada, M. Ehara, K. Toyota, R. Fukuda, J. Hasegawa, M. Ishida, T. Nakajima, Y. Honda, O. Kitao, H. Nakai, M. Klene, X. Li, J.E. Knox, H.P. Hratchian, J.B. Cross, C. Adamo, J. Jaramillo, R. Gomperts, R.E. Stratmann, O. Yazyev, A.J. Austin, R. Cammi, C. Pomelli, J.W. Ochterski, P.Y. Ayala, K. Morokuma, G.A. Voth, P. Salvador, J.J. Dannenberg, V.G. Zakrzewski, S. Dapprich, A.D. Daniels, M.C. Strain,

O. Farkas, D.K. Malick, A.D. Rabuck, K. Raghavachari, J.B. Foresman, J.V. Ortiz, Q. Cui, A.G. Baboul, S. Clifford, J. Cioslowski, B.B. Stefanov, G. Liu, A. Liashenko, P. Piskorz, I. Komaromi, R.L. Martin, D.J. Fox, T. Keith, M.A. Al-Laham, C.Y. Peng, A. Nanayakkara, M. Challacombe, P.M.W. Gill, B. Johnson, W. Chen, M.W. Wong, C. Gonzalez, and J.A. Pople, *Gaussian 03, Revision C.02*, Gaussian, Inc., Wallingford, CT, 2004.

[21] Y.N. Panchenko, *Vibrational spectra and scaled quantum-mechanical molecular force fields*, J. Mol. Struct. 567–568 (2001), pp. 217–230.

[22] G. Rauhut and P. Pulay, *Transferable scaling factors for density functional derived vibrational force fields*, J. Phys. Chem. 99 (1995), pp. 3093–3100.

[23] M.T. Güllüoğlu, Y. Erdogdu, J. Karpagam, and N. Sundaraganesan ve Ş. Yurdakul, *DFT, FT-Raman, FT-IR and FT-NMR studies of 4-phenylimidazole*, J. Mol. Struct. 990 (2011), pp. 14–20.

[24] D. Michalska, *Raint Program*, Wroclaw University of Technology, 2003.

[25] D. Michalska and R. Wysokinski, *The prediction of Raman spectra of platinum (II) anticancer drugs by density functional theory*, Chem. Phys. Lett. 403 (2005), pp. 211–217.

[26] A.E. Reed, L.A. Curtiss, and F. Weinhold, *Intermolecular interactions from a natural bond orbitaldonorndash;acceptor viewpoint*, Chem. Rev. 98 (1998), pp. 899–926.

[27] E.D. Glendening, J.K. Badenhoop, A.E. Reed, J.E. Carpenter, J.A. Bohmann, C.M. Morales, and F. Weinhold, *NBO 5.0*, Theoretical Chemistry Institute, University of Wisconsin, Madison, 2001.

[28] B. Smith, *Infrared Spectral Interpretation: A Systematic Approach*, CRC Press, Washington DC, 1999.

[29] F.R. Dollish, W.G. Fateley, and F.F. Bentley, *Characteristic Raman Frequencies of Organic Compounds*, John Wiley & Sons, New York, 1997.

[30] N.B. Colthup, L.H. Daly, and S.E. Wiberley, *Introduction to Infrared and Raman Spectroscopy*, Academic Press, New York, 1990.

[31] G. Varsanyi, *Vibrational Spectra of Benzene Derivatives*, Academic Press, New York, 1969.

[32] R.G. Pearson, *Absolute electronegativity and hardness correlated with molecular orbital theory*, Proc. Natl Acad. Sci. 83 (1986), pp. 8440–8441.

[33] H. Sklenar and J. Jager, *Molecular structurebiological activity relationships on the basis of quantum chemical calculations*, Int. J. Quantum. Chem. 26 (1979), pp. 467–484.

[34] Z. Zhou and R.G. Parr, *Activation hardness: new index for describing the orientation of electrophilic aromatic substitution*, J. Am. Chem. Soc. 112 (1990), pp. 5720–5724.

[35] P. Chinna Babu, N. Sundaraganesan, Ö. Dereli, and E. Türkkan, *FT-IR, FT-Raman spectra, density functional computations of the vibrational spectra and molecular geometry of butylated hydroxy toluene*, Spectrochim. Acta A: Mol. Biomol. Spectrosc. 79 (2011), pp. 562–569.

[36] Ö. Dereli, S. Sudha, and N. Sundaraganesan, *Molecular structure and vibrational spectra of 4-phenylsemicarbazide by density functional method*, J. Mol. Struct. 994 (2011), pp. 379–386.

[37] M.K. Subramanian, P.M. Anbarasan, and S. Manimegalai, *Molecular structure, NMR and vibrational spectral analysis of 2,4-difluorophenol byab initio HF and density functional theory*, J. Raman Spectrosc. 40 (2009), pp. 1657–1663.

[38] V. Krishnakumar, N. Jayamani, R. Mathammal, and K. Parasuraman, *Density functional theory calculations and vibrational spectra of 2-bromo-4-chloro phenol and 2-chloro-4-nitro phenol*, J. Raman Spectrosc. 40 (2009), pp. 1551–1556.

[39] J. Karpagam, N. Sundaraganesan, S. Kalaichelvan, and S. Sebastian, *Anharmonic vibrational analysis of 3,4-diaminopyridine and 3-aminopyridine by density functional theory calculations*, Spectrochim. Acta Part A 76 (2010), pp. 502–512.